Black hole mass and accretion rate of active galactic nuclei with double-peaked broad emission lines

Xue-Bing Wu, F. K. Liu

Department of Astronomy, Peking University, Beijing 100871, China

wuxb@bac.pku.edu.cn; fkliu@bac.pku.edu.cn

ABSTRACT

Using an empirical relation between the broad line region size and optical continuum luminosity, we estimated the black hole mass and accretion rate for 135 AGNs with double-peaked broad emission lines in two samples, one from the SDSS and the other from a survey of radio-loud broad emission line AGNs. With black hole masses in a range from $3\times10^7M_\odot$ to $5\times10^9M_\odot$, these AGNs have the dimensionless accretion rates (Eddington ratios) between 0.001 ad 0.1 and the bolometric luminosity between $10^{43}erg/s$ and $10^{46}erg/s$, both being significantly larger than those of several previously known low-luminosity ($L_{bol}<10^{43}erg/s$) double-peaked AGNs. The optical–X-ray spectra indices, α_{OX}, of these high-luminosity double-peaked AGNs is between 1 and 1.9, systematically larger than that of low-luminosity objects which is around 1. Modest correlations (with Spearman's rank correlation coefficient of 0.60) of the α_{OX} value with the Eddington ratio and bolometric luminosity have been found, indicating that double-peaked AGNs with higher Eddington ratio or higher luminosity tend to have larger α_{OX} value. Based on these results we suggested that the accretion process in the central region of some high-luminosity double-peaked emission line AGNs (especially those with Eddington ratio larger than 0.01) is probably different from that of low-luminosity objects where a well-known ADAF-like accretion flow was thought to exist. It is likely that the accretion physics in some high-luminosity double-peaked AGNs is similar to that in normal Type 1 AGNs, which is also supported by the presence of possible big blue bumps in the spectra of some double-peaked AGNs with higher Eddington ratios. We noticed that the prototype double-peaked emission line AGN, Arp 102B, having black hole mass of $10^8M_\odot$ and dimensionless accretion rate of 0.001, may be an "intermediate" object between the high and low luminosity double-peaked AGNs. In addition, we found an apparent strong anti-correlation between the peak separation of double-peaked profile and Eddington ratio (with Spearman's rank correlation coefficient

of -0.79). But such an anti-correlation is probably induced by a strong correlation between the peak separation and emission line widths and needs to be confirmed by future works. If it is real, it may provide us another clue to understand why double-peaked broad emission lines were hardly found in luminous AGNs with Eddington ratio larger than 0.1.

Subject headings: accretion, accretion disks — black hole physics — galaxies: active — galaxies: nuclei — quasars: emission lines — quasars: general

1. Introduction

A small number of AGNs display double-peaked broad emission line profiles in their optical spectra (Eracleous & Halpern 1994, 2003). These double-peaked emission lines are usually attributed to the line emission from some parts of accretion disks at a distance of several hundreds to thousands gravitational radius R_g (defined as GM_{BH}/c^2 where M_{BH} is the black hole mass) away from the central black hole (Chen, Halpern & Fillippenko 1989; Chen & Halpern 1989; Halpern 1990). The rotation of photoionized materials in the disk naturally results in two (redshifted and blueshifted) peaks of emission lines. Therefore these double-peaked line profiles are often regarded as one of the evidences for the existence of accretion disks in AGNs. Although the disk origin of double-peaked emission lines is mostly favorite, some other alternatives, such as two broad line regions involving supermassive binary black holes (Begelman, Blandford & Rees 1980), a bipolar outflow (Zheng, Binette & Sulentic 1990), and an anisotropic illuminated broad line region (Goad & Wanders 1996), also exist in the literature.

So far about 150 double-peaked broad emission line AGNs have been discovered. In a completed survey, Eracleous & Halpern (1994, 2003) have found 26 double-peaked broad emission line objects from 106 radio-loud AGNs. The double-peaked profiles of 60% of these 26 objects can be well fitted with the Keplerian rotating accretion disk model. Recently Strateva et al. (2003) presented a new sample of 116 double-peaked Balmer line AGNs selected from the Sloan Digital Sky Survey (SDSS). The profiles of most of these objects can be well fitted with the disk emission model, showing that the double-peaked emission lines are probably produced in the disk part with inner radius of several hundreds of R_g and outer radius of several thousands of R_g. Although 76% of the SDSS double-peaked objects are radio-quiet, they are 1.6 times more likely to be radio sources than other AGNs. The luminosities of these SDSS double-peaked sources are medium ($\sim 10^{44} erg/s$) and only 12% of them are classified as LINERs (Strateva et al. 2003). On the other hand, double-peaked broad emission lines have been also found in some nearby galaxies, including NGC

1097 (Storchi-Bergmann, Baldwin & Wilson 1993), M81 (Bower et al. 1996), NGC 4450 (Ho et al. 2000), and NGC 4203 (Shields et al. 2000). These objects are all classified spectroscopically as Type 1 LINERs and have much lower nuclear luminosity ($< 10^{43} erg/s$) and smaller Eddington ratios ($< 10^{-3}$)(Ho et al. 2000). Together with their relatively flat broad band continuum (Optical–X-ray spectral index $\alpha_{OX} = 0.9 - 1.1$, Ho et al. 2000), these properties suggests that the accretion process in the nuclei of these low-luminosity objects may be in a form of advection-dominated accretion flow (ADAF, see Narayan, Mahadevan & Quataert 1998 for a review). However, it is still not clear whether the high-luminosity (with bolometric luminosity $L_{bol} > 10^{43} erg/s$) AGNs with double-peaked broad emission lines have the same accretion physics as the low-luminosity ones. Strateva et al. (2003) have shown that α_{OX} values for SDSS double-peaked AGNs are in the range of 1 to 2, with an average value of 1.4, which is significantly larger than that of low-luminosity double-peaked sources ($\alpha_{OX} \sim 1$) but similar to that of normal type 1 AGNs (Mushotzky & Wandel 1989). This implies that the accretion physics may be different in the high-luminosity and low-luminosity double-peaked AGNs.

To understand better the nature of the double-peaked AGNs, we need to know some fundamental parameters of them, especially the black hole mass and the accretion rate. Unfortunately, these parameters were known only for 4 low-luminosity sources (NGC 1097, M81, NGC4203, NGC 4450) and 3 high-luminosity sources (Arp 102B, Pictor A and 3C390.3) (see Wandel, Peterson & Malkan (1999) for 3C390.3 and Ho et al. (2000) for others). In this paper we estimate the black hole mass and Eddington ratio for 135 double-peaked AGNs in section 2 and compare the different physical properties of high-luminosity and low-luminosity double-peaked AGNs in section 3. We give the summary and discussion of our results in Section 4.

2. Black hole mass and accretion rate estimations

Several methods have been adopted to estimate the central black hole masses of AGNs. With the dynamic methods, black hole masses of several nearby AGNs, including a double peaked source M81 (NGC 3031), have been estimated (Kormendy & Gebhardt 2001). Black hole masses of about 40 bright Seyfert 1 galaxies and nearby quasars have been derived with the reverberation mapping technique (Wandel, Peterson & Malkan 1999; Ho 1999; Kaspi et al. 2000). Shortly after the confirmation of the applicability of a tight relation between the black hole mass and the bulge velocity dispersion to AGNs (Ferrerase et al. 2001; Tremaine et al. 2002), a method of using such a relation to derive the black hole masses of AGNs from the measured central velocity dispersion was suggested and applied to about 70 Seyfert

galaxies (Wu & Han 2001a; Woo & Urry 2002). However, these methods are applicable to only several double-peaked AGNs and there is no estimate of black hole mass for most double-peaked AGNs.

Reverberation mapping studies of 34 AGNs revealed a significant correlation between the broad line region (BLR) size and the optical continuum luminosity (Kaspi et al. 2000), namely,

$$R_{BLR} = 32.9[\frac{L_{5100\mathring{A}}}{10^{44}erg/s}]^{0.7}\ \mathrm{lt-days}. \quad (1)$$

Interestingly, a double-peaked broad line AGN, 3C 390.3 (with $R_{BLR} = 22.9$ lightdays and $L_{5100\mathring{A}} = 6.4 \times 10^{43} erg/s$), is one of these AGNs and its observational data is well consistent with such an empirical relation. This may imply that we can use the R-L relation to estimate the BLR size from the optical continuum luminosity of high-luminosity double-peaked AGNs. On the other hand, the width (FWHM) of Balmer lines can be used to estimate the velocity dispersion of the BLR. Therefore, The virial mass of the central black hole can be estimated with

$$M_{BH} = 1.464 \times 10^5 (\frac{R_{BLR}}{\mathrm{lt-days}})(\frac{V_{FWHM}}{10^3 km/s})^2 M_\odot, \quad (2)$$

where V_{FWHM} is the FWHM value of Balmer emission lines.

In the reverberation mapping studies, both R_{BLR} and V_{FWHM} are measured mostly from the broad H_β emission line. Previous study has shown that there is a relation between the widths of H_α and H_β emission lines, namely $V_{FWHM}(H_\alpha) = 0.873 V_{FWHM}(H_\beta)$ (Eracleous & Halpern 1994). Kaspi et al. (2000) also derived a linear relation $R_{BLR}(H_\alpha) = 1.19 R_{BLR}(H_\beta) + 13$, which is equivalent to $V_{FWHM}(H_\alpha) = 0.91 V_{FWHM}(H_\beta)$, consistent with the previous result. For the double-peaked AGNs in different samples, usually we have the measurement values of their broad H_α emission line widths. By subtracting the starlight contribution and considering the Galactic extinction, we can also derive the optical continuum luminosity from their apparent magnitudes. Therefore the black hole masses of double-peaked AGNs can be obtained with Eqs. (1) and (2). Assuming a relation between the bolometric luminosity and the optical continuum luminosity, $L_{bol} \simeq 9 L_{5100\mathring{A}}$ (Kaspi et al. 2000), we can estimate their Eddington ratios (defined as $\dot{m} = L_{bol}/L_{Edd}$ where L_{Edd} is the Eddington luminosity given by $L_{Edd} = 1.26 \times 10^{46} erg/s (M_{BH}/10^8 M_\odot)$), which measure the accretion rates of AGNs in Eddington unit. We noticed that the above formula for the conversion between the bolometric luminosity and optical nuclear continuum luminosity was obtained mainly for bright type 1 AGNs, which may not be applicable to all double-peaked AGNs. However, for high-luminosity double-peaked AGNs, the overall SED may not be too different from normal AGNs. Strateva et al. (2003) have shown that the average value of broad band spectral index α_{OX} for the SDSS double-peaked AGNs is similar to normal type

1 AGNs. Only 12% of these SDSS AGNs can be classified as LINERs and most of them may be more similar as luminous broad line AGNs. Therefore, if the starlight contribution is subtracted, the average SED of high-luminosity double-peaked AGNs may be similar to that of type 1 AGNs and the difference in the conversion factor between the bolometric luminosity and nuclear optical continuum luminosity would not significantly change our main results.

Now we apply the method to derive the black hole masses and accretion rates of double-peaked AGNs in the SDSS. Strateva et al. (2003) have given the magnitudes (Galactic extinction corrected), redshifts and FWHM values of the double-peaked H_α line for 109 SDSS AGNs (7 objects have no FWHM values among 116 AGNs in their table 3). From the g and r magnitudes of these AGNs (available in Tables 1 and 2 in Strateva et al. (2003)), we can estimate the rest frame flux at $5100\mathring{A}$ by the following formula:

$$f_{5100\mathring{A}}(Jy) = 3631 \times 10^{-0.4g}[\frac{4770}{5100(1+z)}]^{-\frac{g-r}{2.5lg(6131/4770)}}. \quad (3)$$

Because the starlight fraction values are not available for the SDSS double-peaked AGNs, we assumed a typical value of starlight fraction of double-peaked AGNs as 0.33 (Eracleous & Halpern 2003) to estimate the luminosity of nuclear optical continuum at rest frame $5100\mathring{A}$ (throughout the paper we adopted the Hubble constant as 75 km/s/Mpc and the deceleration parameter as 0.5). Using the conversion formula between the FWHM values of H_α and H_β lines,$V_{FWHM}(H_\alpha) = 0.873V_{FWHM}(H_\beta)$, we can estimate the black hole masses of the double-peaked SDSS AGNs with Eqs (1) and (2). The Eddington ratios of these AGNs can be also derived if we adopted $L_{bol} \simeq 9L_{5100\mathring{A}}$ (Kaspi et al. 2000). The results and the related data of SDSS double-peaked AGNs are summarized in Table 1. We can see that the black hole masses of these double-peaked AGNs are in the range from $4 \times 10^7 M_\odot$ to $5 \times 10^9 M_\odot$, and their Eddington ratios are between 0.002 and 0.2. The average black hole mass of these 109 SDSS double-peaked AGNs is $10^{8.74} M_\odot$ and the average Eddington ratio is $10^{-1.82}$. The histograms of their black hole masses and Eddington ratios are shown in the upper panels of Fig. 1.

The same method is also applied to 26 double-peaked AGNs found from a survey of radio-loud emission line AGNs (Eracleous & Halpern 1994, 2003). Assuming a power-law dependence of continuum flux on the frequency, $f_\nu \propto \nu^{-\alpha}$, the rest-frame flux at $5100\mathring{A}$ can be estimated from the V-band magnitude m_V and Galactic extinction A_V (taken from Schlegel, Finkbeiner & Davis 1998) by the following formula:

$$f_{5100\mathring{A}}(erg\ cm^{-2}s^{-1}\mathring{A}^{-1}) = 3.75 \times 10^{-9}[\frac{5500}{5100(1+z)}]^{2-\alpha}10^{-0.4(m_V-A_V)}. \quad (4)$$

Using the values of V-band magnitude, redshift, starlight fraction of these 26 double-peaked AGNs given in Eracleous & Halpern (1994, 2003)(except that we set the starlight fraction

as 0.9 rather than 1 for MS 0450.3-1817 and Arp 102B in order to estimate the nuclear continuum luminosity), and assuming the spectral index α as about 0.5, we can estimate the nuclear rest-frame continuum luminosity at $5100\mathring{A}$. With the FWHM values of broad H_α line of these AGNs given also in Eracleous & Halpern (1994, 2003) and adopting the conversion formula between the FWHM values of H_α and H_β lines, we can estimate the black hole masses and Eddington ratios of these 26 double-peaked AGNs. The results and the related data are summarized in Table 2. The black hole masses are from $3 \times 10^7 M_\odot$ to $3 \times 10^9 M_\odot$ and the Eddington ratios are between 0.001 and 0.08, The average black hole mass of these 26 double-peaked AGNs is $10^{8.78} M_\odot$ and the average Eddington ratio is $10^{-2.01}$, both being similar to those obtained for the double-peaked SDSS AGNs. The histograms of the black hole masses and Eddington ratios of these 26 radio-loud double-peaked AGNs are shown in the lower panels of Fig. 1.

The black hole masses and Eddington ratios of 3 of the radio-loud, double-peaked AGNs have been estimated previously. For 3C 390.3, the black hole mass of $3.7{\times}10^8 M_\odot$ and Eddington ratio of 0.012 were derived from the reverberation mapping study (Wandel et al. 1998; Kaspi et al. 2000). Our estimation gives the values of $7.3{\times}10^8 M_\odot$ and 0.007 respectively. For Arp 102B and Pictor A, Ho et al. (2000) gave their black hole masses of $2.2{\times}10^8 M_\odot$ and $6.2{\times}10^8 M_\odot$, and Eddington ratios of 0.001 and 0.015 respectively. Our estimations give the black hole mass of Arp 102B as $1.4{\times}10^8 M_\odot$ and that of Pictor A as $5.9{\times}10^8 M_\odot$, the Eddington ratio of Arp 102B as 0.0014 and that of Pictor A as 0.002. Most of our estimated values are consistent with previous results within a factor of a few.

3. Comparison of high-luminosity and low-luminosity AGNs with double-peaked broad emission lines

Double-peaked broad emission line objects have been found in some nearby galaxies, including NGC 1097 (Storchi-Bergmann, Baldwin & Wilson 1993), M81 (Bower et al. 1996), NGC 4203 (Shields et al. 2000) and NGC 4450 (Ho et al. 2000). These objects are all classified spectroscopically as Type 1 LINERs and have very small nuclear luminosity ($< 10^{43} erg/s$), very low Eddington ratios ($< 10^{-3}$) and relatively flat broad band continuum ($\alpha_{OX} = 0.9 - 1.1$) (Ho et al. 2000). However, the high-luminosity AGNs with double-peaked broad emission lines seem to have some different properties from their low-luminosity counterparts. Eracleous & Halpern (1994, 2003) indicated that the X-ray luminosities of most double-peaked objects in their radio-loud sample are larger than $10^{43} erg/s$, implying that the nuclear luminosities of these objects are at least two orders higher than the low-luminosity double-peaked objects. Strateva et al. (2003) also noticed that most double-peaked SDSS

AGNs have optical luminosities of a few times $10^{44} erg/s$, similar to the average value of all SDSS AGNs. They found that only 12% of these double-peaked AGNs are classfied as LINERs. The avearge value of α_{OX} of these objects is 1.4, which is the same as that found for normal type 1 AGNs (Mushotzky & Wandel 1989) and normal SDSS AGNs (Anderson et al. 2003), but significantly larger than that of low-luminosity double-peaked AGNs. These differences between the high-luminosity and low-luminosity double-peaked AGNs may not be purely attributed to the selection effects.

After deriving the black hole masses and Eddington ratios for the high-luminosity double-peaked AGNs in two samples, we are able to compare these fundamental parameters with those of low-luminosity double-peaked objects, which were summarized in Ho et al. (2000). In Fig. 2 we show the values of black hole masses and Eddington ratios of these double-peaked AGNs. Clearly we see that all the 4 low-luminosity objects have black hole masses smaller than $10^8 M_\odot$ and Eddington ratios lower than 10^{-3}, while most of high-luminosity objects have black hole masses larger than $10^8 M_\odot$ and all of them have Eddington ratios higher than 10^{-3}. The average value of black hole masses of high-luminosity objects is about one order larger than that of the low-luminosity objects, and the average value of Eddington ratios of the former objects is about two orders higher than the later ones. We also noticed that the prototype object of double-peaked AGNs, Arp 102B, with black hole mass of $10^{8.1} M_\odot$ and Eddington ratio of $10^{-2.8}$, locates right between the low-luminosity and high-luminosity objects in Fig. 2, meaning that it may be an "intermediate" object. In Fig 3 we show the distributions of the bolometric luminosities of these double-peaked AGNs. We can see that the low-luminosity double-peaked AGNs have both lower bolometric luminosities and lower Eddington ratios, in contrary to the high-luminosity objects. The average value of bolometric luminosities of high-luminosity objects is more than two orders higher than that of low-luminosity objects. Again, Arp 102B, with the bolometric luminosity of $2.7 \times 10^{43} erg/s$, locates right between these low-luminosity and high-luminosity double-peaked AGNs in Fig. 3.

As we have mentioned, there are also differences in the optical–X-ray α_{OX} spectral indices of high and low luminosity double-peaked AGNs. This may reflect the difference in their broad band continuum shapes, which are closely related to the radiation processes in the center of these AGNs. The α_{OX} values are available for 47 SDSS double-peaked AGNs (Strateva et al. 2003) and 4 low-luminosity ones (Ho et al. 2000). Using our estimated nuclear luminosity at $5100\mathring{A}$ (see section 2) and the X-ray luminosity data (mostly in the 0.1-2.4keV band) for 26 double-peaked AGNs in the radio-loud AGN sample (Eracleous & Halpern 2003), we can derive the luminosity values at $2500\mathring{A}$ and 2keV and then estimate the α_{OX} values for these objects assuming a typical optical continuum spectral index of 0.5 and a typical X-ray photon index of 2. The derived α_{OX} values, in a range from 1 to 1.7

and with an average value of 1.2, are also listed in Table 2. Evidently, the α_{OX} values of double-peaked AGNs in two high-luminosity samples are larger than those of low-luminosity objects. In Fig. 4 we show the dependence of α_{OX} value on the Eddington ratio for all these 77 double-peaked AGNs. A Spearman's rank test gives the correlation coefficient of 0.60 and a chance probability of 3.5×10^{-8}, indicating a modest correlation between the α_{OX} values and Eddington ratios. From Fig. 4 we can clearly observe a trend that the objects with lower Eddington ratios seem to have smaller α_{OX} values. When the Eddington ratio of an object is higher than 0.01, it usually has α_{OX} value larger than 1. We noticed that one of the SDSS double-peaked AGNs, SDSS J1710+6521, with the largest Eddington ratio of $10^{-0.9}$ in the SDSS sample, also has the largest α_{OX} value of 1.9. However, we noticed that both the α_{OX} and Eddington ratio depend on the optical continuum luminosity. If we keep the continuum luminosity at $5100\mathring{A}$ fixed, the partial correlation coefficient between the α_{OX} and Eddington ratio is only 0.24. Therefore, the modest correlation between the α_{OX} and Eddington ratio is probably induced by the correlation between the α_{OX} and optical continuum luminosity (or bolometric luminosity), which showes a Spearman's rank corrleation coefficient of 0.60 and a chance probability of 3.2×10^{-8} for 77 double peaked AGNs.

The differences in the Eddington ratios and α_{OX} values of these double-peaked AGNs with high and low luminosities may be also related to the presence or absence of a big blue bump in the optical/UV continuum. Such a big blue bump is usually regarded as the signature of Type 1 AGNs (Sun & Malkan 1989), and most probably originates from the thermal radiation of an optically thick, geometrically thin accretion disk (Shakura & Sunyaev 1973). In Fig. 5 we show the sample spectra of four objects in the SDSS sample of double-peaked AGNs[1]. Two of them, SDSS J1710+6521 and SDSS J1424+5953, have the largest Eddington ratios in the sample, while the other two AGNs, SDSS J0817+3435 and SDSS J0759+3528, have the smallest Eddington ratios. From their spectra we can clearly see that two AGNs with larger Eddington ratios have relatively stronger radiation in the blue-ward of $5000\mathring{A}$ than other two with smaller Eddington ratios. Such a difference in the spectra shape can be also clearly seen from their $u-r$ colors. The $u-r$ values are 0.10 and 0.13 for SDSS J1710+6521 and SDSS J1424+5953, while those are 2.53 and 0.92 for SDSS J0817+3435 and SDSS J0759+3528 respectively. Therefore it is clear that a big blue bump is probably present in some high-luminosity double-peaked AGNs with larger Eddington ratio. The properties of these high-luminosity objects may be similar to type 1 AGNs in many aspects. On the contrary, the low-luminosity double-peaked AGNs, most of which have Eddington ratio lower than 10^{-3}, probably be lack of such a big blue bump in their LINER-like spectra (Ho et al. 2000).

[1]Spectra kindly available from Dr. I. V. Strateva at http://astro.Princeton.EDU/ iskra/original.spectra.tgz

From our study we see the there is only one object with bolometric luminosity larger than $10^{46} erg/s$ and with Eddington ratio larger than 0.1. It seems that we can hardly observe such an object in more luminous AGNs. In some previous studies it has been suggested the reason for that is probably due to the face-on orientation (Corbin 1997) or the broad emission lines arising from an accretion-disk wind rather than from the disk itself (Murray & Chiang 1997; Eracleous & Halpern 2003) for majority of luminous AGNs. Here we propose another explanation based on the investigation of the dependence of the peak separation of the double-peaked emission line profile on the Eddington ratio. Strateva et al. (2003) have given the red peak and blue peak positions, λ_{red} and λ_{blue}, for 116 double-peaked SDSS AGNs in their Table 3. The Eddington ratios of 109 of these objects (other 7 objects have no published FWHM values) have been estimated by us in Section 2. In Fig. 6 we show the relation between the peak separation, $\Delta\lambda = \lambda_{blue} - \lambda_{red}$ (their values are listed in Table 1), and the Eddington ratio for these 109 double-peaked SDSS AGNs. Clearly we see that as the Eddington ratio increases the peak separation decreases. A Spearman's rank test gives a correlation coefficient of -0.79 and a chance probability of 5.2×10^{-24}, suggesting a strong apparent anti-correlation between the peak separation and Eddington ratio. If the Eddington ratio of a double-peaked AGN is higher than 0.1, its peak separation will be probably smaller than 1000km/s (or 22Å). The double peaks in the emission line profile of this object will be very difficult to be detected.

However, we noticed that there is a strong correlation between the line peak separation and line width (FWHM) (with a Spearman's rank correlation coefficient of 0.84). This may natually lead to an anti-correlation between the line peak separation and Eddington ratio because the black hole mass is proportional to the square of FWHM. Keeping the H_β line FWHM fixed, we found the partial correlation coefficient of line peak separation with the Eddington ratio is only 0.05. Therefore, we need to be cautious about such an apparent anti-correlation if we calculate the black hole mass using the emission line width. On the other hand, many studies have shown that narrow line Seyfert 1 galaxies may have relatively smaller black hole masses and higher accretion rates (Boller, Brandt & Fink 1996; Mathur 2000; Puchnarewicz et al. 2001), which seems to support the anti-correlation between the line width the Eddington ratio. Future works, especially those on estimating the black hole mass without using the emission line width, are needed to confirm such an anti-correlation. If it is real, such an anti-correlation may provide us a clue to explain why the double-peaked broad emission line profiles were mostly found in AGNs with low Eddington ratios.

4. Summary and Discussion

We have derived the black hole masses and Eddington ratios for 135 double-peaked broad line AGNs in two samples(Strateva et al. 2003); Eracleous & Halpern 1994, 2003). These estimations enable us to compare their properties with those of several low-luminosity double-peaked AGNs known previously (Ho et al. . 2000). We found that these 135 double-peaked AGNs have black hole masses from $3 \times 10^7 M_\odot$ to $5 \times 10^9 M_\odot$, dimensionless accretion rates (Eddington ratios) from 0.001 to 0.1. and bolometric luminosities from $10^{43} erg/s$ to $10^{46} erg/s$. These values are significantly larger than those of several low-luminosity AGNs with double-peaked broad emission lines. The optical–X-ray α_{OX} spectral indices of these double-peaked AGNs are from 1 to 1.9, with an average value of 1.4 and 1.2 respectively in two samples, being systematically larger than those of low-luminosity double-peaked AGNs. We have found a modest correlation between the α_{OX} value and Eddington ratio for double-peaked AGNs and have shown that the double-peaked AGNs with higher Eddington ratios (or higher luminosity) tend to have larger α_{OX} values. In addition, we demonstrated the differences in the continuum shape for double-peaked AGNs with higher and lower Eddington ratios and found that the objects with larger Eddington ratios probably display a big blue bump in their spectra, similar to many normal type 1 AGNs. However, an apparent anti-correlation was found between the peak separation and Eddington ratio. If such an anti-correlation could be confirmed by future works, it may help us to explain why the double-peaked profiles are hardly observed in more luminous AGNs with Eddington ratio higher than 0.1.

Our results suggested that high-luminosity double-peaked AGNs probably have some different properties from low-luminosity ones. This is supported by the smaller fraction (12%) of LINER-like objects in the SDSS double-peaked AGNs (Strateva et al. 2003), but is different from the previous suspicion that the double-peaked broad line AGNs are LINER-like objects with low-luminosity and low accretion rate (Eracleous & Halpern 1994; Ho et al. 2000). Now we see that the double-peaked broad emission lines can also be found in AGNs with bolometric luminosity up to $10^{46} erg/s$, with black hole mass up to $10^9 M_\odot$ and with Eddington ratio up to 0.1. Some high luminosity double-peaked AGNs, especially those with Eddington ratio larger than 0.01, may share many similar properties, such as a big blue bump and a large α_{OX} value, as normal type 1 AGNs. Our results support that the high-luminosity double-peaked AGNs (with Eddington ratio larger than 0.01) may have different accretion disk structure with low-luminosity ones. This can be clearly see from the relation of their α_{OX} values with Eddington ratios (see Fig. 4). Most probably, an ADAF-like accretion flow exists in the low-luminosity double-peaked AGNs with Eddington ratio smaller than 0.01 while an optically thick, geometrically think accretion disk exists in the high-luminosity double-peaked AGNs with Eddington ratios larger than 0.01. Such a critical Eddington ratio

or dimensionless accretion rate (around 0.01) has been also mentioned in some theoretical studies on the transition between the hot ADAF and the cold disk models(Esin, McClintock & Narayan 1997; Narayan et al. 1998; Rozanska & Czerny 2000). The different radiation processes in an ADAF and a cold disk may naturally account for the observed lower α_{OX} values of low-luminosity double-peaked AGNs and the higher values of high-luminosity ones. The absence of a big blue bump in the low-luminosity double-peaked AGNs and the presence of that in some high-luminosity double-peaked AGNs are also consistent with the different accretion process in these objects. However, more detailed theoretical modelings of the accretion disk structure and the broad emission line region of double-peaked AGNs are still needed to understand our derived relations of the α_{OX} value and the peak separation with Eddington ratio.

Finally we would like to mention that there are substantial uncertainties in estimating the black hole masses and Eddington ratios of double-peaked AGNs. Although we believe that considering these uncertainties will not alter the main results in this paper, we should be cautious in using the estimated value of black hole mass and Eddington ratio for a specific object. Firstly, the poor understandings of the geometry and dynamics of the broad line region may cause substantial errors in black hole mass estimation (Krolik 2001). The inclination of the broad line region, which may not be randomly distributed for double-peaked AGNs, may lead to an uncertainty in black hole mass up to a factor of a few (McLure & Dunlop 2001; Wu & Han 2001b). Secondly, the variations of the broad emission line profiles are common in double-peaked AGNs (Zheng, Veilleux & Grandi 1991; Newman et al. 1997; Storchi-Bergmann et al. 2003). This may also affect the accuracy of black hole mass estimation using the Virial law. Thirdly, the starlight fraction for double-peaked AGNs varies a lot from 0.1 to 1 (Eracleous & Halpern 1994). A careful subtractions of the starlight from the observed luminosity must be performed in order to accurately estimate the nuclear continuum luminosity, which is important in deriving the broad line region size and the bolometric luminosity for a double-peaked AGN. Finally, in this paper the bolometric luminosity of double-peaked AGNs is simply derived from the nuclear continuum luminosity at $5100\mathring{A}$. More accurate estimations may be done by integrating the observed flux points in a SED from radio to X-ray or by fitting the average SED for double-peaked AGNs to the available flux points (Woo & Urry 2001). Future efforts in diminishing these uncertainties will be undoubtedly much helpful to understand the physics of double-peaked broad line AGNs.

We are grateful to the anonymous referee for helpful suggestions which improve the presentation of our paper. The work is supported by the National Key Project on Fundamental Researches (TG 1999075403), the National Natural Science Foundation (No. 10173001 and

N0. 10203001) in China .

REFERENCES

Anderson, S.F., et al. 2003, AJ, 126, 2209

Begelman, M.C., Blandford, R.D., & Rees, M.J. 1980, Nature, 287, 307

Boller, Th., Brandt, W. N., & Fink, H. 1996, A&A, 305, 53

Bower,G.A., Wilson, A.S., Hecman, T.M., & Richstone, D.O. 1996, AJ, 111, 1901

Chen, K., & Halpern, J.P. 1989, ApJ, 344, 115

Chen, K., Halpern, J.P. & Filippenko, A.V. 1989, ApJ, 339, 742

Corbin, M. A. 1997, ApJ, 485, 517

Eracleous, M. & Halpern, J.P. 1994, ApJS, 90, 1

Eracleous, M. & Halpern, J.P. 2003, ApJ, 599, 886

Esin, A.A., McClintock, J.E., & Narayan, R. 1997, ApJ, 489, 865

Ferrerase, L., Pogge, R. W., Peterson, B. M., Merritt, D., Wandel, A., Joseph, C. L. 2001, ApJ, 555, L79

Goad, M., & Wanders, I. 1996, ApJ, 469, 113

Halpern, J. P. 1990, ApJ, 365, L51

Ho, L.C. 1999, in Observational Evidence for Black Holes in the Universe, ed S.K. Charkrabarti (Dordrecht: Kluwer), 157

Ho, L. C., Rix, H.-W., Shields, J. C., Rudnick, G., McIntosh, D. H., Filippenko, A. V., & Sargent, W. L. W. , & Eracleous, M. 2000, ApJ, 541, 120

Kaspi, S., Smith, P.S., Netzer, H., Maoz, D., Jannuzi, B.T., & Giveon, U. 2000, ApJ, 533, 631

Kormendy, J. & Gebhardt, K. 2001, in The 20th Texas Symposium on relativistic astrophysics, AIP conference proceedings, Vol. 586. Eds J. Craig Wheeler & Hugo Martel, 363

Krolik, J.H., 2001, ApJ, 551, 72

Mathur. S. 2000, MNRAS, 314, L17

McLure, R.J. & Dunlop, J.S. 2001, MNRAS, 327, 199

Mushotzky, R.F., & Wandel, a. 1989, ApJ, 339, 674

Murray, N., & Chiang, J. 1997, ApJ, 474, 91

Narayan, R., Mahadevan, R. Quataert, E., 1999, In Theory of Black Hole Accretion Disks, eds Abramowicz M., Bjornsson G., & Pringle J., Cambridge University Press

Newman, J. A., Eracleous, M., Filippenko, A. V., & Halpern, J. P. 1997, ApJ, 485, 570

Puchnarewicz, E. M., Mason, K. O., Siemiginowska, A., Fruscione, A., Comastri, A., Fiore, F., & Cagnoni, I. 2001, ApJ, 550, 644

Rozanska, A. & Czerny, B. 2000, A&A, 360, 1170

Shakura, N.I. & Sunyaev, R.A. 1973, A&A, 24, 337

Schlegel, D. J. Finkbeiner, D. P. & Davis, M. 1998, ApJ, 500, 525

Shields, J.C. et al. 2000, ApJ, 534, L27

Storchi-Bergmann, T., Baldwin, J. A., & Wilson, A. S. 1993, ApJ, 410, L11

Storchi-Bergmann, T. et al. 2003, ApJ, 598, 956

Strateva I., et al. 2003, AJ, 126 1720

Sun, W.-H., & Malkan, M.A. 1989, ApJ, 346, 68

Tremaine, S. et al. 2002, ApJ, 574, 740

Wandel, A., Peterson, B.M., & Malkan, M.A. 1999, ApJ, 526, 579

Woo, J.-H. & Urry, C.M. 2002, ApJ, 579, 530

Wu, X.-B. & Han, J.L. 2001a, A&A, 380, 31

Wu, X.-B. & Han, J.L. 2001b, ApJ, 561, L59

Zheng, W., Binette, L., & Sulentic, J. W. 1990, ApJ, 365, 115

Zheng, W., Veilleux, S., & Grandi, S. A. 1991, ApJ, 381, 418

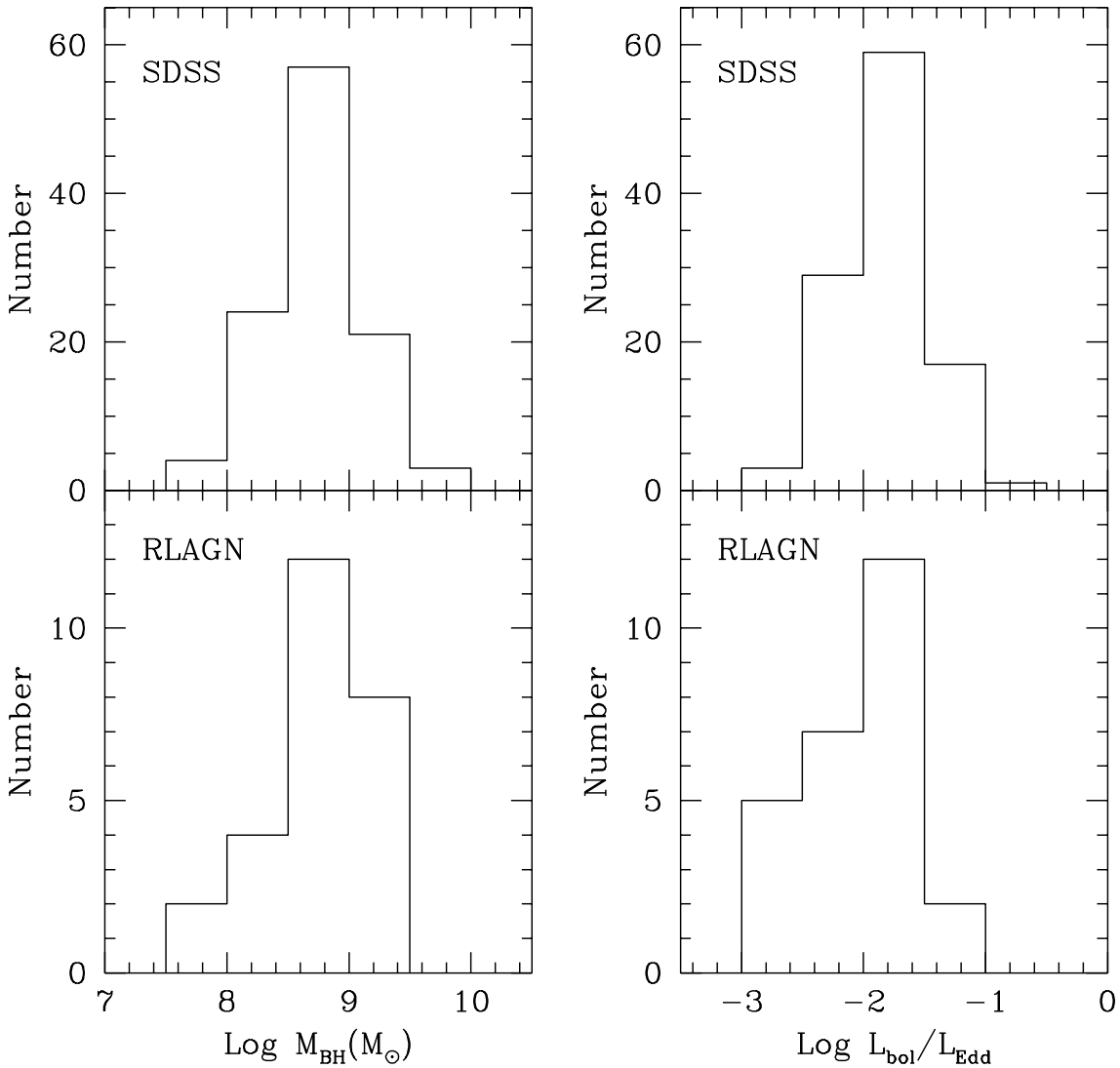

Fig. 1.— The histograms of the black hole masses and Eddington ratios of double-peaked AGNs in the SDSS (Strateva et al. 2003) and radio-loud AGN (Eracleous & Halpern 1994, 2003) samples.

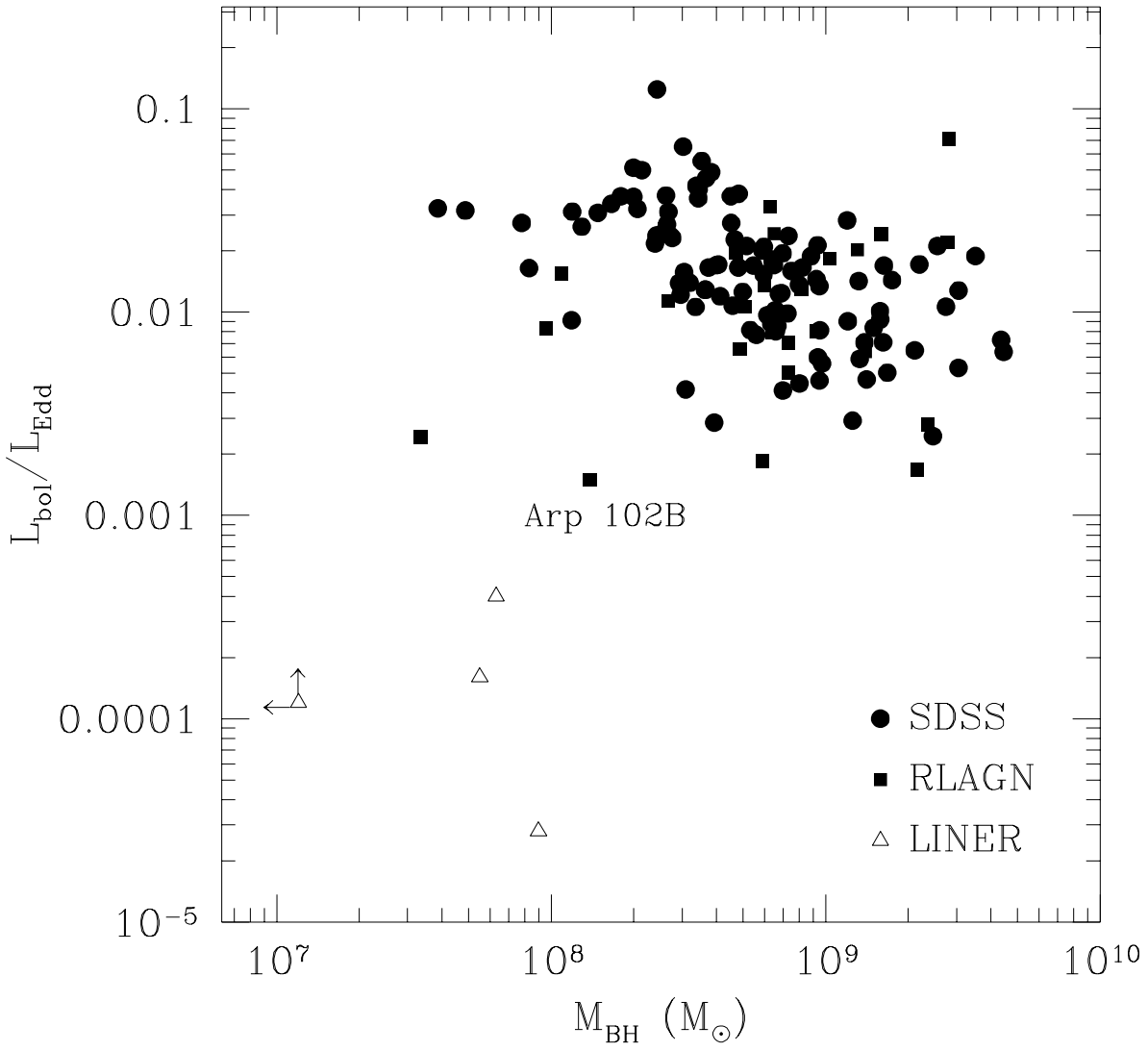

Fig. 2.— Black hole mass Eddington ratio distributions in three different samples of double-peaked AGNs. The solid circles and squares represent the sources in the SDSS (Strateva et al. 2003) and the radio-loud AGN survey (Eracleous & Halpern 1994, 2003) respectively. The open triangles represent four low-luminosity sources spectroscopically identfied as LINERs (Ho et al. 2000).

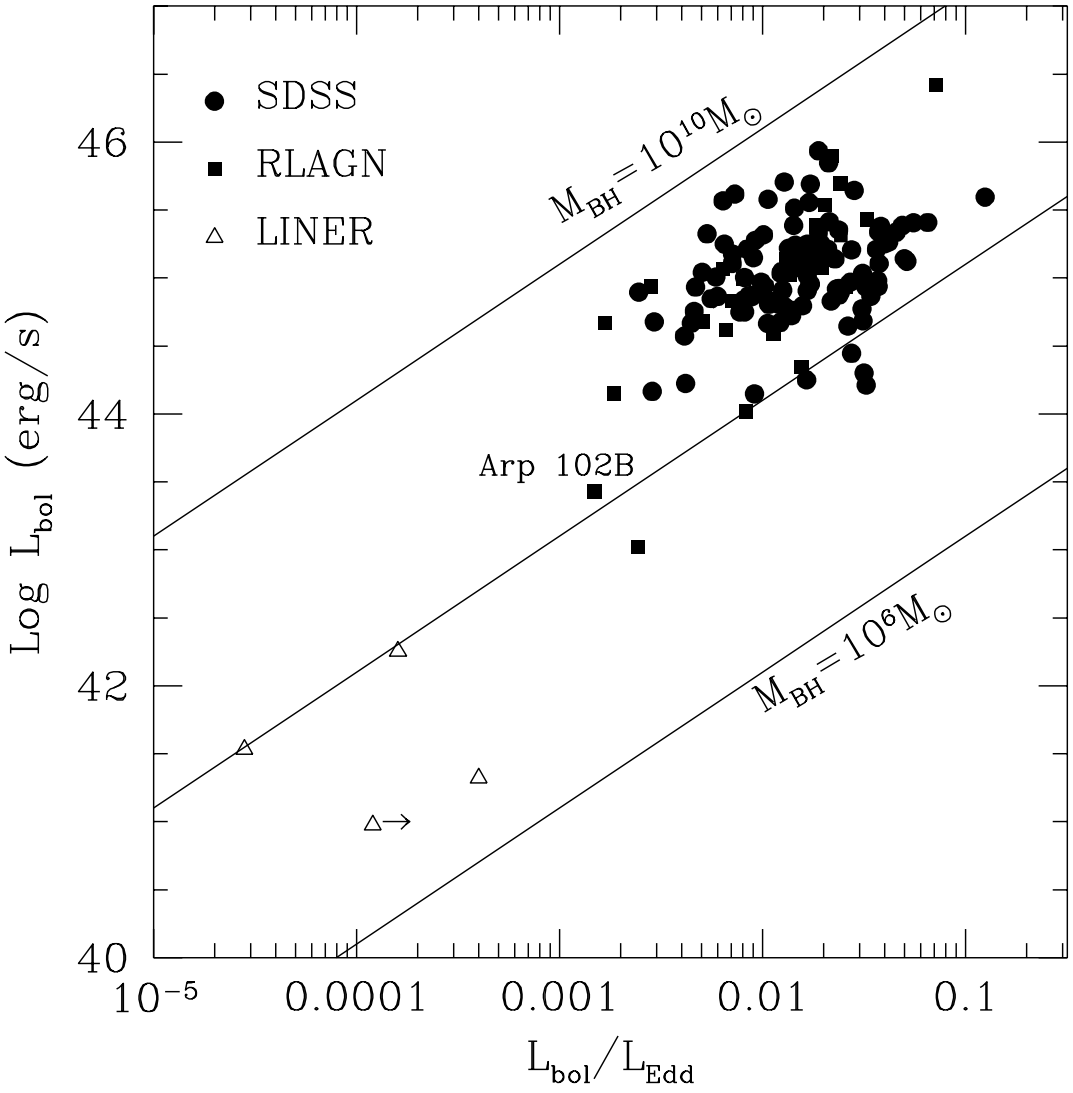

Fig. 3.— Relation between bolometric luminosity and Eddington ratios for three different samples of double-peaked AGNs. The symbols have the same meanings as in Fig. 2. The solid lines represent the relations for the cases with black hole mass of $10^6 M_\odot$, $10^8 M_\odot$ and $10^{10} M_\odot$ respectively.

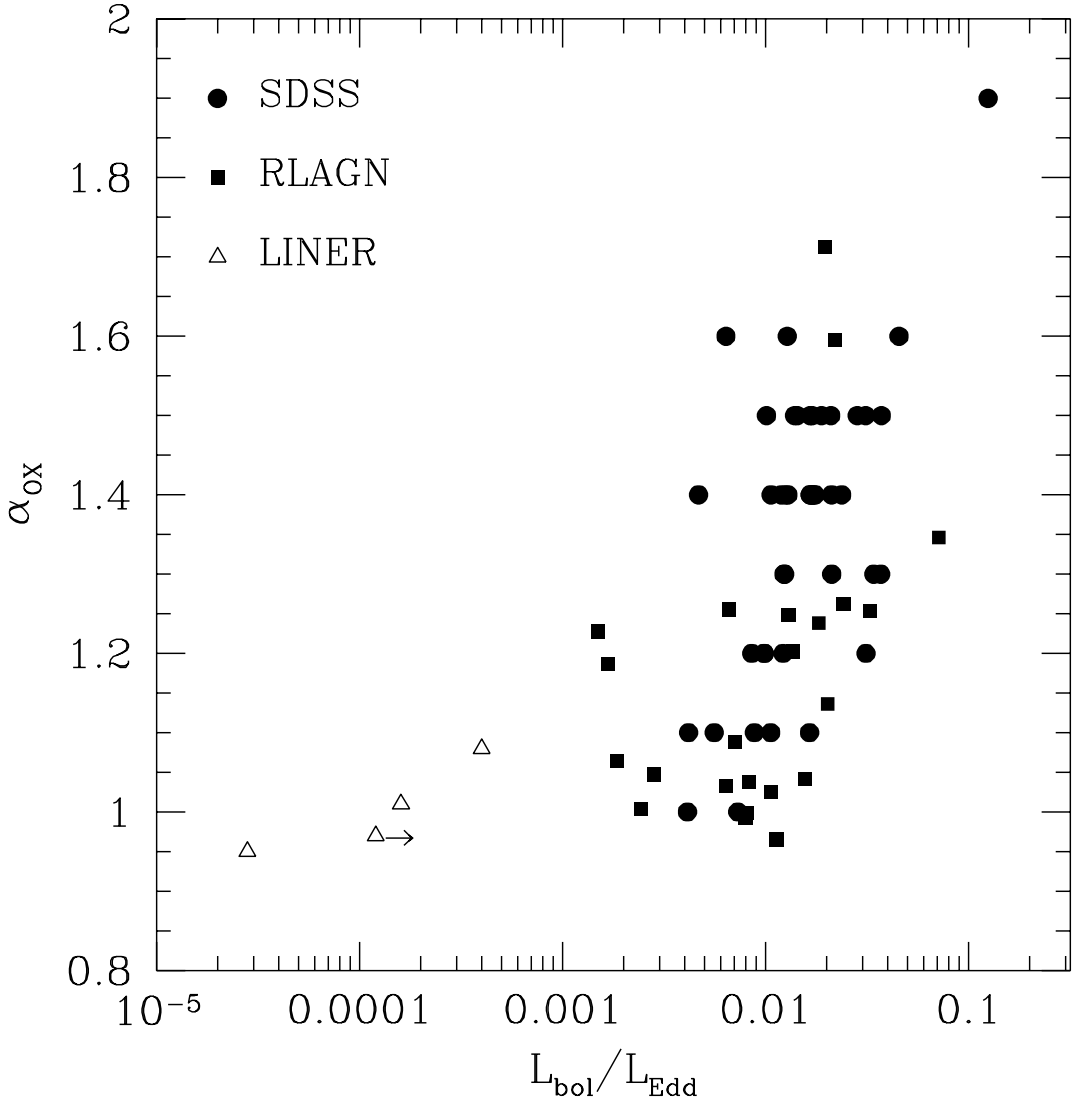

Fig. 4.— Relation between α_{OX} and Eddington ratios for three different samples of double-peaked AGNs. The symbols have the same meanings as in Fig. 2.

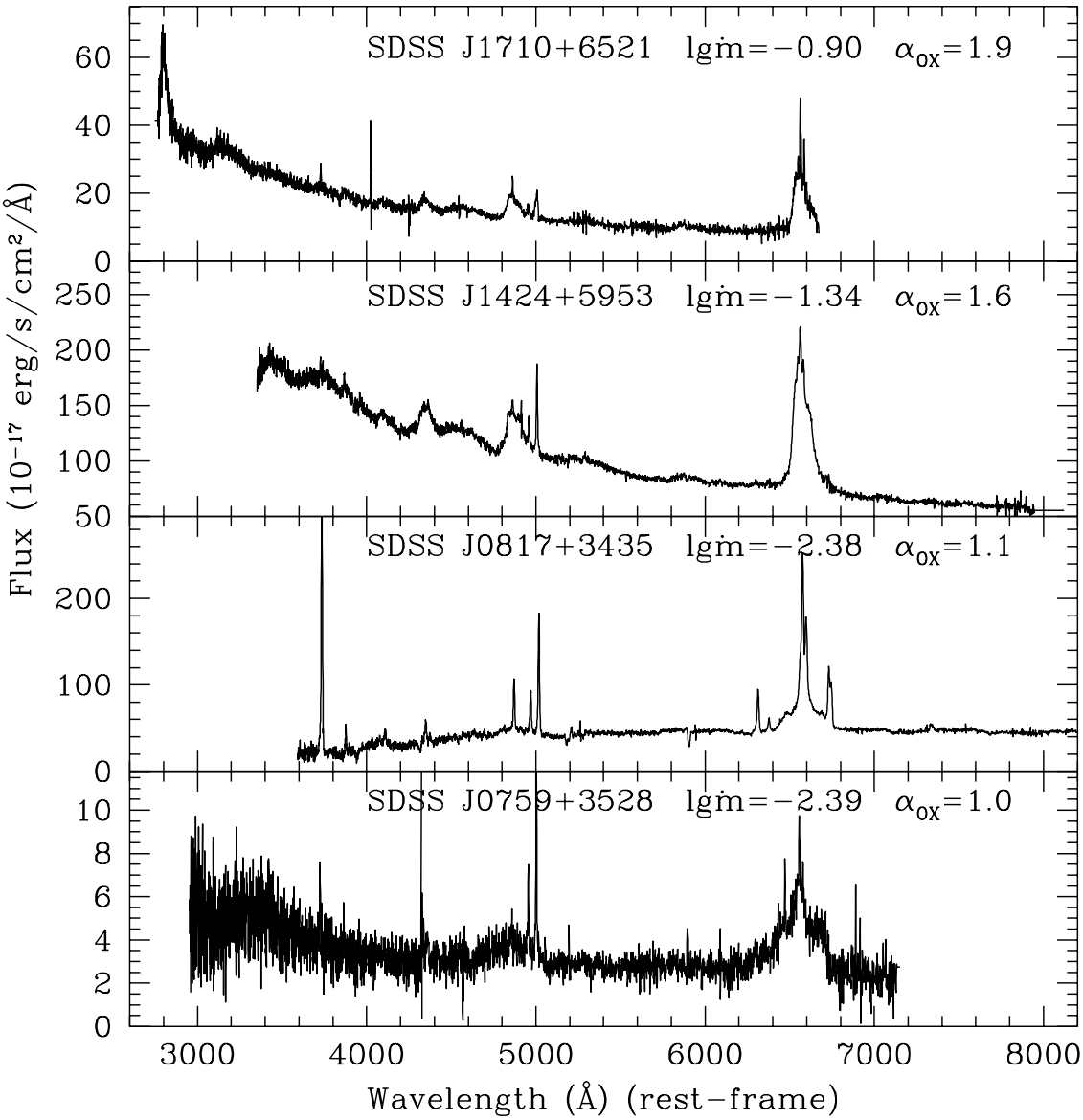

Fig. 5.— Comparison of sample spectra of four double-peaked SDSS AGNs. Two AGNs in the two upper panels have largest Eddington ratios ($\dot{m} = L_{bol}/L_{Edd}$) while two in the two lower panels have smallest Eddington ratios in the SDSS sample.

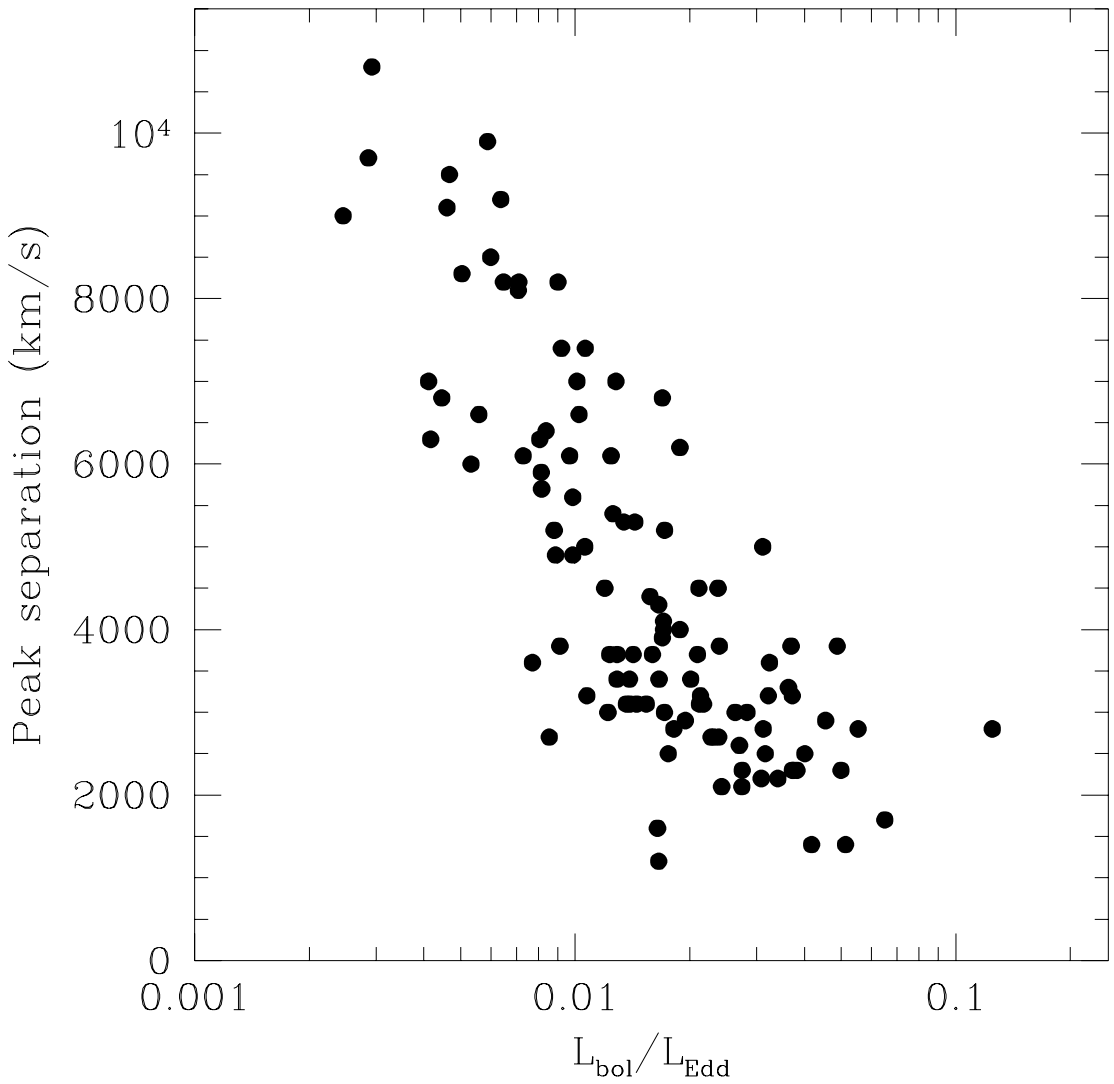

Fig. 6.— The relation between the peak separation in double-peaked broad line profiles and Eddington ratio for the double-peaked SDSS AGNs.

Table 1: Data of 116 double-peaked broad line AGNs in the SDSS sample

Name	z	FWHM (km/s)	$LogL_{5100\mathring{A}}$ (erg/s)	$LogM_{BH}$ ($M_\odot$)	$Log\ \dot{m}$	α_{OX}	Peak separation (km/s)
SDSS J0007+0053	0.3159	9800	44.89	9.408	-1.675	1.4	4500
SDSS J0008-1046	0.1986	9600	44.2	8.903	-1.866	...	3100
SDSS J0012-1022	0.22	5500	44.43	8.584	-1.312	...	3800
SDSS J0043+0051	0.3083	11800	44.36	9.198	-1.995	1.5	7000
SDSS J0057+1446	0.1718	9900	44.6	9.213	-1.771	1.5	3900
SDSS J0111-0958	0.2064	5400	43.98	8.254	-1.43	...	2300
SDSS J0117-0111	0.1855	5600	43.82	8.17	-1.511	...	2200
SDSS J0132-0952	0.2597	15200	44.09	9.225	-2.298	...	8300
SDSS J0134-0841	0.0699	8300	43.19	8.075	-2.04	...	3800
SDSS J0149-0808	0.2093	5400	43.73	8.077	-1.506	1.2	2800
SDSS J0212-0030	0.3942	...	44.63	...	...	...	...
SDSS J0216-0052	0.2778	9600	43.85	8.661	-1.969	...	3200
SDSS J0220-0728	0.2136	6100	44.08	8.427	-1.507	1.5	5000
SDSS J0229-0008	0.6091	...	44.36	...	...	...	...
SDSS J0232-0828	0.2652	8400	44.46	8.971	-1.671	...	3200
SDSS J0240-0041	0.2466	9600	44.29	8.966	-1.839	...	3100
SDSS J0247-0714	0.334	13100	44.15	9.142	-2.149	...	8100
SDSS J0248-0100	0.184	6800	43.97	8.441	-1.636	...	2700
SDSS J0252+0043	0.1696	6400	44.01	8.423	-1.569	...	2600
SDSS J0259-0015	0.1018	4500	43.26	7.587	-1.49	...	3600
SDSS J0300-0714	0.3883	...	44.92	...	...	...	...
SDSS J0325+0008	0.3602	12000	44.75	9.485	-1.893	1.6	7000
SDSS J0349-0626	0.2877	9900	44.26	8.977	-1.872	...	5300
SDSS J0739+4043	0.2081	14200	43.71	8.905	-2.351	...	6800
SDSS J0741+2755	0.3256	5700	44.31	8.529	-1.379	...	1400
SDSS J0754+4316	0.3475	10300	44.74	9.342	-1.765	1.4	5200
SDSS J0759+3528	0.2886	14300	43.62	8.844	-2.386	1	7000
SDSS J0803+2932	0.3277	9700	44.09	8.839	-1.906	1.3	6100
SDSS J0806+4841	0.37	12600	44.62	9.438	-1.974	1.4	7400
SDSS J0813+4834	0.2738	8400	44.23	8.807	-1.741	...	2800
SDSS J0817+3435	0.062	12600	43.27	8.49	-2.38	1.1	6300
SDSS J0819+4817	0.2228	9200	43.96	8.698	-1.901	1.4	5400
SDSS J0821+3503	0.2936	5000	44.19	8.331	-1.302	...	2300
SDSS J0821+4219	0.222	11200	43.88	8.818	-2.093	...	6300
SDSS J0821+4702	0.1283	10800	43.91	8.802	-2.056	1.1	5200
SDSS J0822+4553	0.2998	6200	44.43	8.683	-1.418	...	2300
SDSS J0824+3342	0.3179	12500	44.26	9.175	-2.077	...	6400
SDSS J0832+3707	0.092	15200	43.98	9.149	-2.331	1.4	9500

Name	z	FWHM (km/s)	$LogL_{5100\mathring{A}}$ (erg/s)	$LogM_{BH}$ ($M_\odot$)	$Log\ \dot{m}$	α_{OX}	Peak separation (km/s)
SDSS J0838+3719	0.211	9200	43.71	8.526	-1.975	1.1	5000
SDSS J0841+0229	0.3322	8300	44.06	8.682	-1.78	1.4	3400
SDSS J0845+0016	0.2613	10600	44.01	8.861	-2.007	1.2	5600
SDSS J0904+5536	0.0372	...	43.03	...	...	...	...
SDSS J0914+0126	0.1977	12200	44.32	9.2	-2.036	...	7400
SDSS J0918+5139	0.1855	4900	44.17	8.3	-1.29	...	1400
SDSS J0925+5317	0.1862	8000	44.23	8.77	-1.697	...	3400
SDSS J0935+4819	0.2237	8500	44.21	8.808	-1.756	1.4	2500
SDSS J0936+5331	0.2281	4800	44.45	8.481	-1.187	...	1700
SDSS J0938+0057	0.1704	8300	44.29	8.844	-1.711	...	2900
SDSS J1000+0259	0.339	10200	44.43	9.121	-1.848	...	3700
SDSS J1004+4801	0.1986	13500	43.89	8.987	-2.253	1.1	6600
SDSS J1014+0006	0.1412	20700	43.94	9.392	-2.61	...	9000
SDSS J1027+6050	0.3314	16200	44.61	9.649	-2.196	1.6	9200
SDSS J1032+6008	0.2939	7900	44.26	8.775	-1.679	1.5	3700
SDSS J1041-0050	0.3029	7800	44.4	8.864	-1.625	1.4	4500
SDSS J1041+0232	0.182	10800	43.8	8.725	-2.088	...	5700
SDSS J1041+5620	0.2304	13100	43.91	8.972	-2.222	...	8500
SDSS J1107+0421	0.3269	9000	44.24	8.876	-1.797	...	3700
SDSS J1127+6750	0.194	5500	43.91	8.22	-1.468	1.3	2200
SDSS J1130+0058	0.1325	6900	44.25	8.656	-1.562	...	2100
SDSS J1130+0222	0.241	6000	44.26	8.536	-1.44	...	3300
SDSS J1136+0207	0.239	5800	44.3	8.538	-1.397	...	2500
SDSS J1140+0546	0.1315	14400	43.8	8.977	-2.337	...	9100
SDSS J1143-0029	0.1715	10300	43.99	8.817	-1.99	...	6600
SDSS J1150-0316	0.1486	10800	43.92	8.81	-2.052	...	4900
SDSS J1152+6048	0.2703	10400	43.96	8.806	-2.007	1.2	4900
SDSS J1156+6147	0.2265	5700	44.15	8.419	-1.427	...	2300
SDSS J1211+6044	0.637	...	44.24	...	...	1.1	...
SDSS J1218+0200	0.327	7900	44.69	9.079	-1.549	1.5	3000
SDSS J1220-0132	0.2879	8800	44.12	8.774	-1.813	...	3100
SDSS J1238+5325	0.3478	15400	44.66	9.639	-2.137	1	6100
SDSS J1309+0322	0.2665	8000	44	8.609	-1.766	...	3000
SDSS J1324+0524	0.1154	14900	43.21	8.595	-2.543	...	9700
SDSS J1328-0129	0.1515	11100	43.8	8.748	-2.113	...	3600
SDSS J1333+0130	0.2171	8700	43.83	8.56	-1.891	...	3400
SDSS J1333+0418	0.2022	8000	43.99	8.603	-1.768	1.4	4100
SDSS J1334-0138	0.2917	16300	44.37	9.484	-2.274	...	6000
SDSS J1339+6139	0.3723	13400	44.22	9.209	-2.148	...	8200

Name	z	FWHM (km/s)	$LogL_{5100\mathring{A}}$ (erg/s)	$LogM_{BH}$ ($M_\odot$)	$Log\ \dot{m}$	α_{OX}	Peak separation (km/s)
SDSS J1346+6220	0.1163	...	43.93	...	...	1.6	...
SDSS J1351+6531	0.2988	8400	44.13	8.737	-1.771	1.4	6800
SDSS J1400+6314	0.3309	10600	44.56	9.242	-1.843	1.5	5300
SDSS J1407+0235	0.3094	13900	44.05	9.124	-2.23	...	9900
SDSS J1414+0133	0.2704	11000	43.92	8.825	-2.068	1.2	2700
SDSS J1416+0219	0.158	11800	44.05	8.979	-2.089	...	5900
SDSS J1419+6503	0.1478	6600	43.92	8.384	-1.623	...	2700
SDSS J1424+5953	0.1348	5600	44.38	8.564	-1.342	1.6	2900
SDSS J1427+6354	0.1453	9100	43.85	8.616	-1.923	1.4	4500
SDSS J1434+5723	0.1749	7700	44.2	8.712	-1.674	1.3	3100
SDSS J1521+0337	0.1261	6600	43.95	8.403	-1.615	...	2100
SDSS J1540-0205	0.32	10700	44.98	9.546	-1.725	...	6200
SDSS J1545+5736	0.2681	7400	44.19	8.669	-1.643	...	2700
SDSS J1605-0109	0.2425	6700	43.97	8.432	-1.621	...	3800
SDSS J1635+4816	0.3088	8000	43.95	8.573	-1.781	1.5	1200
SDSS J1638+4335	0.3391	9000	44.29	8.915	-1.781	1.4	4300
SDSS J1701+3404	0.0945	6400	43.3	7.92	-1.784	1.1	1600
SDSS J1710+6521	0.3853	3700	44.64	8.386	-0.9043	1.9	2800
SDSS J1718+5933	0.2728	10400	43.93	8.788	-2.015	...	6100
SDSS J1721+5344	0.1918	8200	43.77	8.466	-1.857	1.5	3400
SDSS J1727+6322	0.2175	8700	44.38	8.947	-1.725	1.5	4000
SDSS J1730+5500	0.2491	6800	43.88	8.379	-1.663	...	3100
SDSS J2050-0701	0.1686	5500	44.03	8.3	-1.433	1.3	3800
SDSS J2101-0547	0.1794	9700	44.08	8.83	-1.91	1.3	3700
SDSS J2113-0612	0.2411	5800	43.69	8.111	-1.58	...	3000
SDSS J2125-0813	0.6246	...	45.36	...	...	1.2	...
SDSS J2145+1210	0.1113	5300	43.49	7.893	-1.562	...	2300
SDSS J2149+1138	0.2393	17600	43.72	9.098	-2.534	...	10800
SDSS J2150-0010	0.3351	6200	44.39	8.655	-1.43	1.5	3200
SDSS J2221-0109	0.2878	14400	44.3	9.325	-2.188	...	8200
SDSS J2229+0008	0.2657	5200	44.45	8.549	-1.257	...	2800
SDSS J2233-0743	0.175	8300	43.81	8.504	-1.856	...	3100
SDSS J2233-0843	0.0582	4700	43.35	7.687	-1.501	...	2500
SDSS J2304-0841	0.0471	8600	43.72	8.472	-1.914	1.2	3000
SDSS J2305-0036	0.2687	11800	44.2	9.081	-2.046	...	8200
SDSS J2312-0116	0.2139	5800	43.98	8.315	-1.493	...	3200
SDSS J2327+1524	0.046	7900	43.84	8.485	-1.803	...	4400
SDSS J2332+1513	0.2146	8600	44.2	8.812	-1.768	...	4000
SDSS J2351+1552	0.0966	8700	43.83	8.562	-1.89	1.4	3700

Table 2: Data of 26 double-peaked broad line AGNs in the radio-loud AGN sample

Name	z	m_V	A_V	SF[a]	FWHM (km/s)	$LogL_{5100\mathring{A}}$ (erg/s)	$LogM_{BH}$ ($M_\odot$)	$Log\ \dot{m}$	α_{OX}
3C 17	0.22	18	0.077	0.58	11500	43.66	8.687	-2.182	1.255
4C 31.06	0.373	18	0.175	0.11	9000	44.44	9.014	-1.738	1.238
3C 59	0.109	16	0.211	0.28	9800	44.18	8.912	-1.888	1.248
PKS 0235+023	0.209	17.7	0.109	0.46	11200	43.87	8.805	-2.099	0.9925
IRAS 02366–3101	0.063	14.98	0.218	0.30	7800	44.13	8.673	-1.707	1.712
PKS 0340–37	0.285	18.6	0.032	0.19	9800	43.89	8.708	-1.975	1.025
3C 93	0.357	19.2	0.804	0.43	19600	43.98	9.372	-2.551	1.09
MS 0450.3–1817	0.059	17.8	0.144	0.90	10900	42.07	7.523	-2.615	1.047
Pictor A	0.035	16.2	0.142	0.14	18400	43.2	8.769	-2.731	1.064
B2 0742+31	0.462	16	0.227	0	6500	45.46	9.451	-1.147	1.346
CBS 74	0.092	16	0.118	0.17	9200	44.07	8.776	-1.867	1.203
PKS 0857–19	0.36	19.7	0.685	0	6500	43.98	8.415	-1.591	...
PKS 0921–213	0.053	16.5	0.2	0.65	8300	43.06	7.983	-2.08	1.038
PKS 1020–103	0.197	16.1	0.153	0	8700	44.74	9.201	-1.616	1.262
4C 36.18	0.392	18	0.056	0	6800	44.48	8.798	-1.483	1.254
PKS 1151–34	0.258	17.8	0.284	0.75	13400	43.73	8.864	-2.297	...
TXS 1156+213	0.349	17.5	0.088	0.43	7600	44.36	8.812	-1.615	...
CSO 643	0.276	16.7	0.042	0.28	9000	44.58	9.116	-1.694	1.136
3C 303	0.141	17.3	0.063	0.73	6800	43.39	8.039	-1.808	1.138
3C 332	0.151	16	0.079	0.85	23200	43.72	9.334	-2.776	1.269
Arp 102B	0.024	14.8	0.08	0.90	16000	42.48	8.141	-2.826	1.286
PKS 1739+18C	0.186	17.5	0.206	0.11	13600	44.11	9.144	-2.195	1.033
3C 382	0.059	15.4	0.231	0.31	11800	44.04	8.969	-2.094	0.9985
3C 390.3	0.057	15.4	0.237	0.31	11900	43.87	8.864	-2.149	1.183
PKS 1914–45	0.368	16.8	0.266	0.10	9800	44.95	9.446	-1.659	1.595
PKS 2300–18	0.129	17.8	0.108	0.14	8700	43.64	8.427	-1.948	0.9648

[a] Starlight fraction values were taken from Eracleous & Halpern (1994, 2003) except that a value of 0.9 instead of 1 was adopted for MS 0450.3-1817 and Arp 102B.